Experimental Investigation of Vibrating Laminated Composite Plates by Optical Interferometry Method

Chien-Ching Ma* and Chan-Chiao Lin†

National Taiwan University, Taipei 10617, Taiwan, Republic of China

Most of the work done for the vibration of composite plates published in the literature are analytical and numerical studies with few experimental results available. In this study, an experimental amplitude-fluctuation electronic speckle pattern interferometry method for out-of-plane displacement measurement is employed to investigate the vibration behavior of square and rectangular composite plates with different stacking sequences. Both resonant frequencies and corresponding mode shapes can be obtained experimentally using the present method. High-quality interferometric fringes for mode shapes are produced instantly by a video recording system. Four different types of geometric configurations and stacking sequences of 16-layer laminated composite plates are investigated in this study, namely, a $[0]_{16}$ square plate, a $[0]_{16}$ rectangular plate, a $[0/45/90/-45]_{2s}$ square plate, and a $[0/45/90/-45]_{2s}$ rectangular plate. The numerical calculations by the finite element method and Rayleigh–Ritz technique are performed, and the results are compared with the experimental measurements. Good agreement is obtained for both results of resonant frequencies and mode shapes.

Nomenclature

D_{ij} = laminate bending stiffness
w = transverse displacement
λ = wavelength of laser
ρ = mass density
ω = vibration frequency

Introduction

HOLOGRAPHIC interferometry opened new worlds of research by making possible accurate, global measurement of small dynamic surface displacements in a two-step process for a wide variety of objects. For this purpose, different methods of holographic interferometry, which have made possible the gathering of a large amount of information, have been developed for vibration analysis. Unfortunately, the slow and cumbersome process of film development limits the application of holographic vibration analysis. Electronic speckle pattern interferometry (ESPI) was proposed in the 1970s (Ref. 1) as a method of producing the interferogram without using traditional film-based techniques.[2] As compared with the traditional holographic interferometry, the interferometric fringe patterns of ESPI are recorded using a video camera, thus eliminating the chemical film development process. Because the interferometric image is recorded and updated every $\frac{1}{30}$ s, ESPI is faster and more insensitive to environment than holography. For these reasons, ESPI has become a powerful technique used in many academic research and engineering applications. Because ESPI uses video recording and display, its real-time nature makes it practical for vibration measurement. The most widely used experimental setup to study vibration by ESPI is the time-averaged method.[3] The disadvantage of this method is that the interferometric fringes represent only the amplitude, but not the phase, of the vibration. Løkberg and Hogmoen[4] developed the phase-modulation method, which used the reference beam modulation technique to determine the relative phase of the vibrating object. To reduce the noise coming from the environment, the subtraction method was developed,[5,6] where the reference frame is first recorded before vibration and continuously subtracted from the incoming frames after vibration. However, the interferometric fringe visibility of the subtraction method is not good enough for quantitative measurement of surface displacement. To increase the visibility of the fringe pattern and to reduce the environmental noise

simultaneously, an amplitude-fluctuation ESPI (AF-ESPI) method was proposed by Wang et al.[7] for out-of-plane vibration measurement. In the AF-ESPI method, the reference frame is recorded in a vibrating state and subtracted from the incoming frame. Consequently, it combines the advantages of the time-averaged and subtraction methods, that is, good visibility and noise reduction. Ma and Huang[8] and Huang and Ma[9] used the AF-ESPI method to investigate the three-dimensional vibrations of piezoelectric rectangular parallelepipeds and cylinders. Both the resonant frequencies and the mode shapes were presented and discussed in detail.

Modern engineering design requires the use of materials in a way that optimizes their inherent properties. The general class of materials that is most suitable for optimum design is composites. Composite materials are increasingly being used in many engineering applications for a variety of reasons, such as high specific stiffness and weight reduction. Composite structural elements are now used in a variety of components for automotive, aerospace, marine, and architectural structures, in addition to consumer products. Fiber-reinforced laminated composites are the most popular because of their ability to offer outstanding strength, stiffness, low specific gravity, and unique flexibility, which satisfy the requirements of a large number of structural applications. Structures made of advanced composites, such as fiber-reinforced plastics, often consist of a number of layers having unidirectional fibers.

The problem of determining the resonant frequencies of laminated plates has been studied extensively in the literature, and most of the published works include analytical and numerical results. However, there are very few experimental results available, especially for the full-field measurement of vibration mode shapes. In this paper, we employ an optical method based on AF-ESPI to investigate experimentally the resonant properties (resonant frequencies and mode shapes) of composite laminated plates. The advantage of using the AF-ESPI method is that both resonant frequencies and the corresponding mode shapes can be obtained simultaneously from the experimental measurement. The fringe patterns shown in the experiment correspond to the vibration mode shapes. Good quality of the interferometric fringe patterns for the mode shapes are provided for the free vibration of laminated plates. In the analysis of a nonhomogeneous multilayered composite plate, it is common to treat the multilayered composite plate as a single homogeneous plate with effective or homogenized material constants. We construct the effective laminate bending stiffness for composite plates from an averaging process of the material properties of lamina, and the material constants are used for numerical investigations. Finally, numerical computations based on a finite element package are also presented, and good agreement of resonant frequencies and mode shapes are found for both results.

*Professor, Department of Mechanical Engineering.
†Graduate Student, Department of Mechanical Engineering.

Vibration of Composite Plates

For a laminated plate with midplane symmetry, there is no extensional–bending coupling, and the in-plane response can be assumed to be negligible compared with the flexure-induced displacement. For a symmetric laminate plate subjected to bending only, the laminate moment–curvature relationships are given by

$$\begin{Bmatrix} M_x \\ M_y \\ M_{xy} \end{Bmatrix} = \begin{bmatrix} D_{11} & D_{12} & D_{16} \\ D_{12} & D_{22} & D_{26} \\ D_{16} & D_{26} & D_{66} \end{bmatrix} \begin{Bmatrix} k_x \\ k_y \\ k_{xy} \end{Bmatrix} \tag{1}$$

where (M_x, M_y, M_{xy}) and (k_x, k_y, k_{xy}) are the moment and the curvature, respectively. D_{ij} $(i, j = 1, 2, 6)$ is the flexural stiffness.

The partial differential equation governing the transverse motion of a symmetrically laminated thin plate is

$$D_{11}\frac{\partial^4 w}{\partial x^4} + 4D_{16}\frac{\partial^4 w}{\partial x^3 \partial y} + 2(D_{12}+D_{66})\frac{\partial^4 w}{\partial x^2 \partial y^2} + 4D_{26}\frac{\partial^4 w}{\partial x \partial y^3}$$

$$+ D_{22}\frac{\partial^4 w}{\partial y^4} = -\rho h \frac{\partial^2 w}{\partial t^2} \tag{2}$$

For the orthotropic plate, we have $D_{16} = D_{26} = 0$. For free harmonic vibrations at frequency ω, we can assume that

$$w(x, y, t) = W(x, y)\sin\omega t \tag{3}$$

where $W(x, y)$ is the maximum deflection and can be represented as a linear series of assumed functions:

$$W(x, y) = \sum_{m=1}^{p}\sum_{n=1}^{q} A_{mn} X_m(x) Y_n(y) \tag{4}$$

The assumed functions $X_m(x)$ and $Y_n(y)$ must be admissible, such that they satisfy the essential boundary conditions of the plate. The characteristic equations of vibrating beams are used as the assumed functions X_m and Y_n. The characteristic equations of vibrating beams are chosen so that the boundary conditions of the beam matches those of the plate, guaranteeing satisfaction of the essential boundary conditions. The method of determining the set of characteristic functions and a summary of the properties of these functions was given by Young.[10] The characteristic functions $X_m(x)$ for the free–free beam used in this study are given as follows:

$$X_1(x) = 1, \qquad X_2(x) = \sqrt{3}[1 - (2x/\ell)]$$

$$X_m(x) = \cosh(c_m x/\ell) + \cos(c_m x/\ell) - \alpha_m[\sinh(c_m x/\ell)$$

$$+ \sin(c_m x/\ell)], \qquad m = 3, 4, 5, \ldots$$

where ℓ is the length of the beam. The numerical values of c_m and α_m are given by Young.[10] The functions $X_1(x)$ and $X_2(x)$ represent a rigid-body translation and rotation, respectively, and are included to obtain a complete orthogonal set. Similar expressions also are used for $Y_n(y)$. With the stationary potential energy theory, the Rayleigh–Ritz technique will provide a discrete number of stationary values ω_s, which are the lowest upper bounds of the actual resonant frequencies.[11]

T300/976 graphite/epoxy composite plates with stacking sequences $[0/45/90/-45]_{2s}$ and $[0]_{16}$, respectively, and an isotropic aluminum 6061-T6 plate are evaluated in this study. The material properties of the graphite/epoxy lamina and the aluminum are indicated in Table 1, where E_1 and E_2 are Young's moduli in the longitudinal and transverse directions, respectively; G_{12} is the in-plane shear modulus; and ν_{12} is Poisson's ratio of the lamina. To simplify the problem, the nonhomogeneous multilayered laminated composite plate is usually treated as a single homogeneous layer with effective material constants by an averaging process. The averaging process is performed as follows: 1) Form the stiffness coefficients for the

Table 2   Dimensions of the tested plates

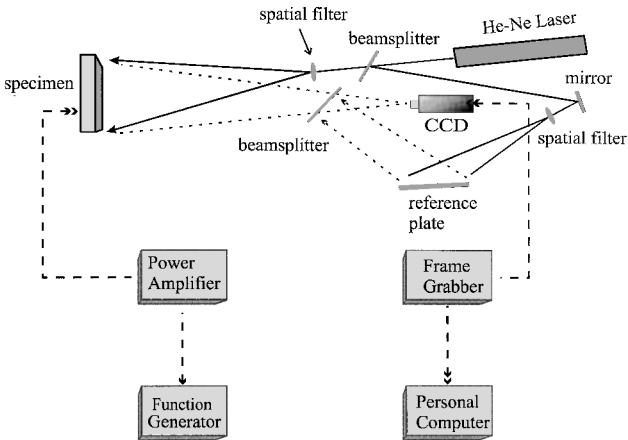| Plate	a, mm	b, mm	h, mm
Aluminum square plate	80	80	1
$[0]_{16}$ Square plate	99	99	2
$[0]_{16}$ Rectangular plate	99	52	2
$[0/45/90/-45]_{2s}$ Square plate	102	102	2
$[0/45/90/-45]_{2s}$ Rectangular plate	102	51	2

Fig. 1   Schematic diagram of ESPI setup for out-of-plane measurement.

lamina. 2) Use tensor transformation for each lamina to obtain transformed lamina stiffness matrix for different fiber orientation. 3) Construct the laminate bending stiffness. The laminate bending stiffness for $[0]_{16}$ and $[0/45/90/-45]_{2s}$ laminate plates are obtained from the material properties of lamina shown in Table 1, and the results for $[0]_{16}$ are $D_{11} = 93.46$ GPa·mm³, $D_{12} = 1.87$ GPa·mm³, $D_{22} = 6.52$ GPa·mm³, and $D_{66} = 3.72$ GPa·mm³ and for $[0/45/90/-45]_{2s}$ are $D_{11} = 50.88$ GPa·mm³, $D_{12} = 10.14$ GPa·mm³, $D_{16} = D_{26} = 3.56$ GPa·mm³, $D_{22} = 32.55$ GPa·mm³, and $D_{66} = 11.98$ GPa·mm³. The dimensions of the tested plates are shown in Table 2.

Experimental and Numerical Results

The basic theory of the AF-ESPI method for out-of-plane vibration measurement can be found in Refs. 7–9. The schematic layout of a self-arranged AF-ESPI optical system, as shown in Fig. 1, is employed to perform the out-of-plane vibration measurement of the resonant frequencies and mode shapes for composite plates. A He–Ne laser with 30 mW and wavelength $\lambda = 632.8$ nm is used as the coherent light source. The laser beam is divided into two parts, the reference and object beams, by a beamsplitter. We use a charge-coupled device (CCD) camera (Pulnix Company) and a P360F (Dipix Technologies, Inc.) frame grabber with Digital Signal Processor (DSP) onboard to record and process the images. The object beam travels to the specimen and then reflects to the CCD camera. The reference beam is directed to the CCD camera via the mirror and reference plate. Note that the optical path and the light intensity of these two beams should remain identical in the experimental setup. The CCD camera converts the intensity distribution of the interference pattern of the object into a corresponding video signal at 30 frames per second. The signal is electronically processed and finally converted into an image on the video monitor. The interpretation of the fringe image is similar to reading a contour map. To increase the intensity of light reflection of the specimens and the contrast of fringe patterns, the surfaces of the plates are coated with white paint, which is mixed with fine seaweed powder. The plate is excited by the piezostack actuator (Physik Instrumente; $5 \times 5 \times 10$ mm), which is attached to the specimen. The piezoelectric actuator is usually attached by adhesive in the center of the opposite face of the specimen. However, if the nodal lines pass the center of the specimen, then the piezoelectric actuator will be

Table 1   Material constants of the tested plates

Material	E_1, GPa	E_2, GPa	G_{12}, GPa	ν_{12}	ν_{21}	ρ, kg/m³
Graphite/epoxy	139.3	9.72	5.586	0.29	0.02	1550
Aluminum	70	70	26	0.33	0.33	2700

moved to another location. To achieve the sinusoidal output, a function generator HP33120A (Hewlett Packard) connected to a 4005 power amplifier (NF Electronic Instruments) is used.

The experimental procedure of the AF-ESPI technique is performed as follows. First, a reference image is taken after the specimen vibrates, then the second image is taken, and the reference image is subtracted by the image processing system. If the vibrating frequency is not the resonant frequency, only randomly distributed speckles are displayed and no fringe patterns will be shown. However, if the vibrating frequency is in the neighborhood of the resonant frequency, stationary distinct fringe patterns will be observed. Then the function generator is carefully and slowly turned; the number of fringes will increase and the fringe pattern will become clearer as the resonant frequency is approached. From the aforementioned experimental procedure, the resonant frequencies and the corresponding mode shapes can be determined at the same time using the AF-ESPI optical system.

Composite and isotropic aluminum plates with all edges free are used to have the ideal boundary conditions for theoretical and experimental simulations. The resonant frequency and the correspondent mode shape for the vibrating plate are determined experimentally using the noncontacting optical method of AF-FSPI. The numerical predictions of resonant frequencies and mode shapes are carried out by using the commerically available finite element package ABAQUS[12] in which nine-node two-dimensional shell elements (S9R5) are used to analyze the problem. Furthermore, a FORTRAN program in which equations are derived by the Rayleigh–Ritz technique is also used to predict the resonant frequencies.

To verify the procedure described, an isotropic aluminum square plate is evaluated. The material properties and dimensions of the aluminum plate are listed in Tables 1 and 2, respectively. The results presented in Table 3 show generally good agreement between the predicted and measured resonant frequencies. The error in resonant frequency prediction is given by

$$\%\text{Error} = \frac{(f_{\text{exp}} - f_{\text{predicted}})}{f_{\text{predicted}}} \times 100\%$$

The percentage errors between the experimental data and the analytical Rayleigh–Ritz and finite element results are also shown in Table 3. The largest error is 6.6% and the average error in the results is 4%. The errors may be due to thickness variations across the plate, the material property measurement, the experimental determination of resonant frequencies, and errors in finite element and Rayleigh–Ritz solutions. However, the differences between the finite element and Rayleigh–Ritz results are generally less than 1%.

Figure 2 shows the first six mode shapes of an isotropic aluminum square plate for both experimental measurements and numerical simulations. For the finite element calculations, the contours of constant displacement for resonant mode shapes are plotted to compare with the experimental observation. In Fig. 2, we indicate the phase of displacement in finite element results as a solid or a dashed line, where the solid lines are in the opposite direction from the dashed lines. The boundaries separating the solid lines and dashed lines are the nodal lines. The zero-order fringe, which is the brightest fringe on the experimental image, represents the nodal lines of the vibrating

AF-ESPI   FEM   AF-ESPI   FEM

Mode 1 (2,2)   Mode 4

Mode 2   Mode 5
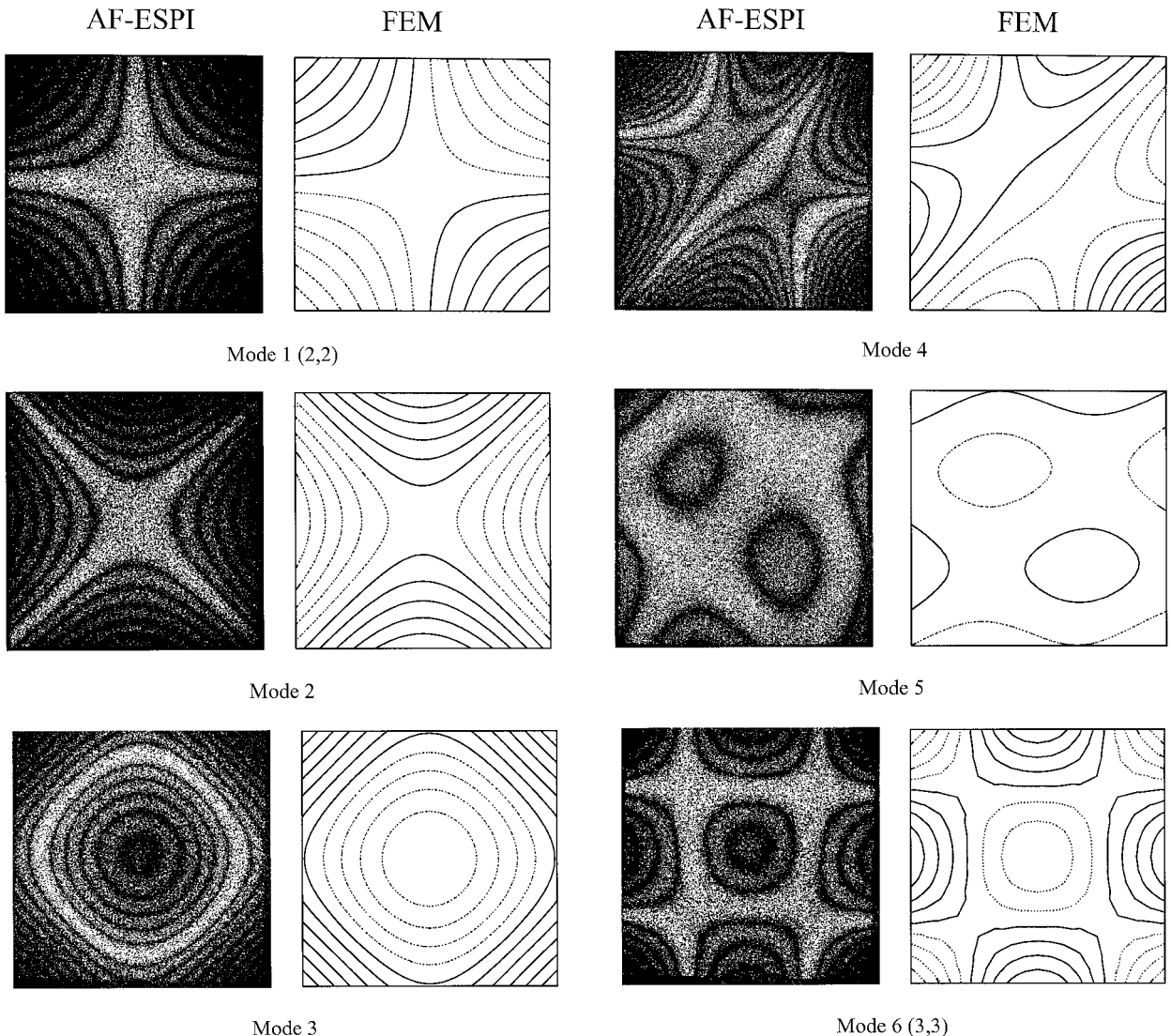
Mode 3   Mode 6 (3,3)

Fig. 2   First six mode shapes for isotropic aluminum square plate obtained from experimental observation and numerical calculation.

Table 3   Results of resonant frequencies obtained from Rayleigh–Ritz method, FEM, and AF-ESPI for the square aluminum plate

Mode number (index)	Results of resonance, Hz	FEM		AF-ESPI	
		Hz	Error, %	Hz	Error, %
1 (2,2)	509	510	0.20	494	−2.95
2	755	746	−1.19	735	−2.65
3	953	945	−0.84	890	−6.61
4	1334	1322	−0.90	1271	−4.72
5	2381	2358	−0.97	2330	−2.14
6 (3,3)	2447	2428	−0.78	2345	−4.17

plate at resonant frequencies. The rest of the fringes are contours of constant amplitudes of displacement. The excellent quality of the experimental fringe patterns for vibration mode shapes of the isotropic square plate are also presented in Fig. 2. The mode shapes obtained by experimental results can be checked by comparing the nodal lines and fringe patterns with the numerical finite element calculations, and excellent agreements are found. Extensive experimental results of the resonant frequencies and mode shape for isotropic plates with two different types of boundary conditions were obtained by Huang and Ma.[13] A digital speckle pattern interferometry technique was developed by Slangen et al.[14] and was applied to study the resonant frequencies and mode shapes of a cantilever aluminum plate.

Because of the symmetry of the geometric configuration of the isotropic square plate and the boundary condition, two possible mode shapes may exist at the same resonant frequency. If the plate is
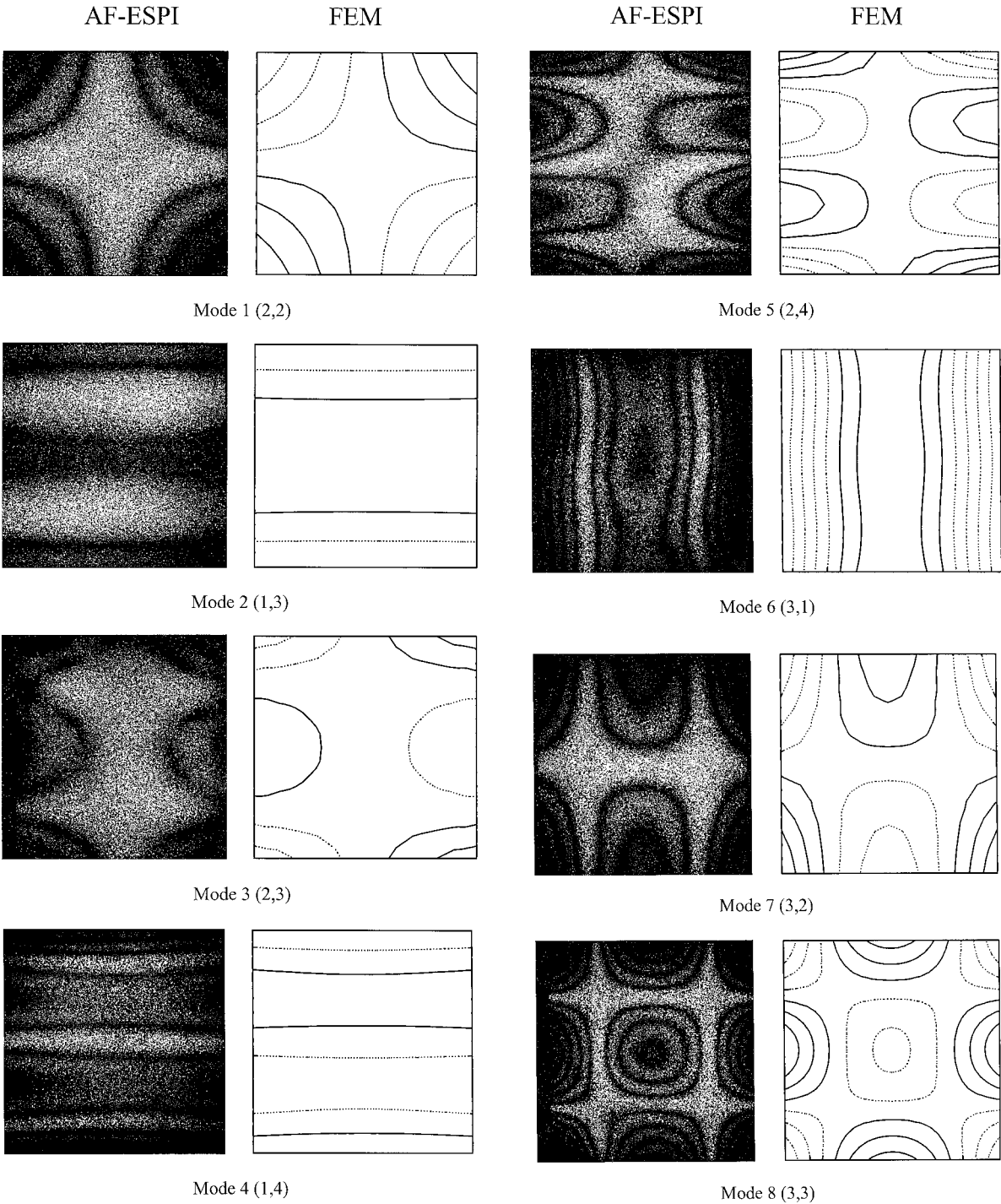

AF-ESPI   FEM

Mode 1 (2,2)

Mode 2 (1,3)

Mode 3 (2,3)

Mode 4 (1,4)

AF-ESPI   FEM

Mode 5 (2,4)

Mode 6 (3,1)

Mode 7 (3,2)

Mode 8 (3,3)

Fig. 3   First eight mode shapes for [0]₁₆ composite square plate obtained from experimental observation and numerical calculation (also appears in Ref. 15).

Table 4 Results of resonant frequencies obtained from Rayleigh–Ritz method, FEM, and AF-ESPI for the $[0]_{16}$ square composite plate

Mode number (index)	Results of resonance, Hz	FEM		AF-ESPI	
		Hz	Error, %	Hz	Error, %
1 (2,2)	409	407	−0.49	400	2.20
2 (1,3)	526	525	−0.19	501	−4.75
3 (2,3)	991	985	−0.61	1003	1.21
4 (1,4)	1449	1445	−0.28	1466	1.17
5 (2,4)	1916	1900	−0.84	1856	−3.13
6 (3,1)	1993	1977	−0.80	1958	−1.76
7 (3,2)	2157	2137	−0.93	2134	−1.07
8 (3,3)	2661	2620	−1.54	2609	−1.95

Table 5 Results of resonant frequencies obtained from Rayleigh–Ritz method, FEM, and AF-ESPI for the $[0]_{16}$ rectangular composite plate

Mode number (index)	Results of resonance, Hz	FEM		AF-ESPI	
		Hz	Error, %	Hz	Error, %
1 (2,2)	789	780	−1.14	767	−2.79
2	1884	1876	−0.42	1895	0.58
3	2017	2002	−0.74	2006	−0.55
4 (2,3)	2482	2456	−1.05	2500	0.73
5 (3,2)	2547	2511	−1.41	2516	−1.22
6 (3,3)	4269	4163	−2.48	4120	−3.49
7 (1,4)	5262	5219	−0.82	5292	0.57

Table 6 Results of resonant frequencies obtained from Rayleigh–Ritz method, FEM, and AF-ESPI for the $[0/45/90/-45]_{2s}$ square composite plate

Mode number (index)	Results of resonance, Hz	FEM		AF-ESPI	
		Hz	Error, %	Hz	Error, %
1	671	662	−1.34	654	−2.53
2	1065	1056	−0.85	1028	−3.47
3	1416	1402	−0.99	1355	−4.31
4	1702	1677	−1.47	1636	−3.88
5	1978	1935	−2.17	1891	−4.40
6	3060	3015	−1.47	2891	−5.52
7	3225	3140	−2.64	3079	−4.53

Table 7 Results of resonant frequencies obtained from Rayleigh–Ritz method, FEM, and AF-ESPI for the $[0/45/90/-45]_{2s}$ rectangular composite plate

Mode number (index)	Results of resonance, Hz	FEM		AF-ESPI	
		Hz	Error, %	Hz	Error, %
1	1172	1264	7.85	1178	0.51
2	1514	1389	−8.26	1311	−13.41
3 (3,2)	2921	2948	0.92	2781	−4.79
4	3829	3670	−4.15	3485	−8.98
5	4420	4348	−1.63	4037	−8.67
6	5279	5125	−2.92	4855	−8.03
7 (4,2)	5364	5329	−0.65	5071	−5.46

AF-ESPI   FEM

Mode 1 (2,2)

Mode 2

Mode 3

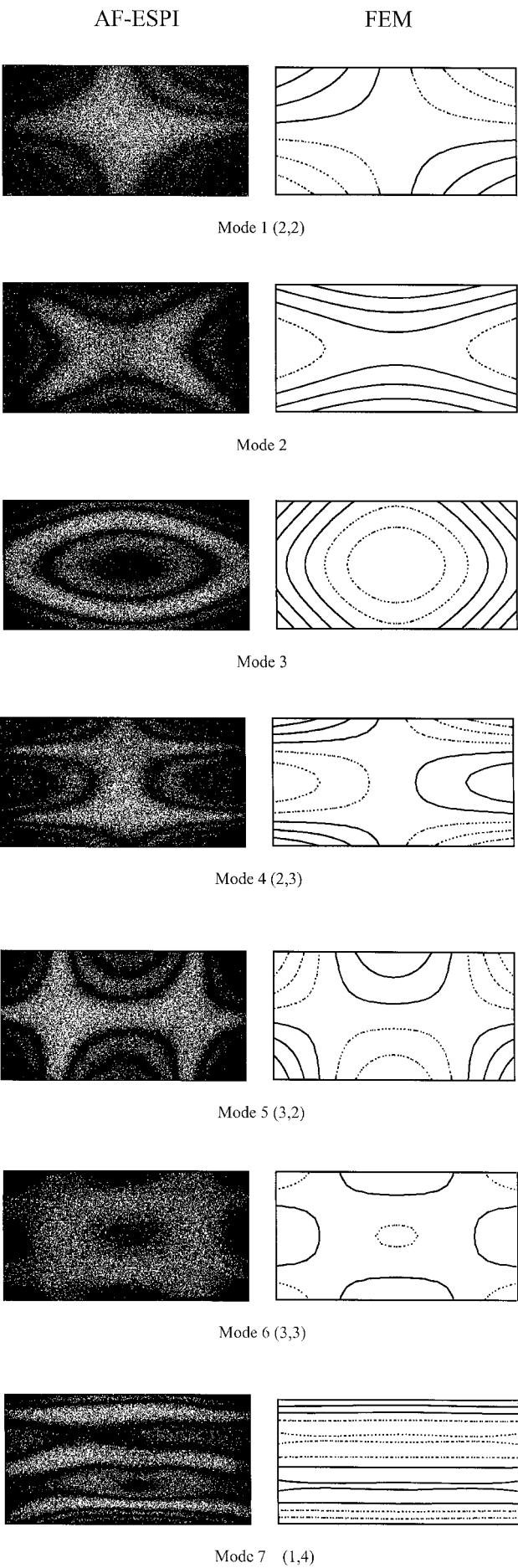

Mode 4 (2,3)

Mode 5 (3,2)

Mode 6 (3,3)

Mode 7 (1,4)

Fig. 4 First seven mode shapes for $[0]_{16}$ composite rectangular plate obtained from experimental observation and numerical calculation.

AF-ESPI   FEM

Mode 1

Mode 2

Mode 3

Mode 4

AF-ESPI   FEM
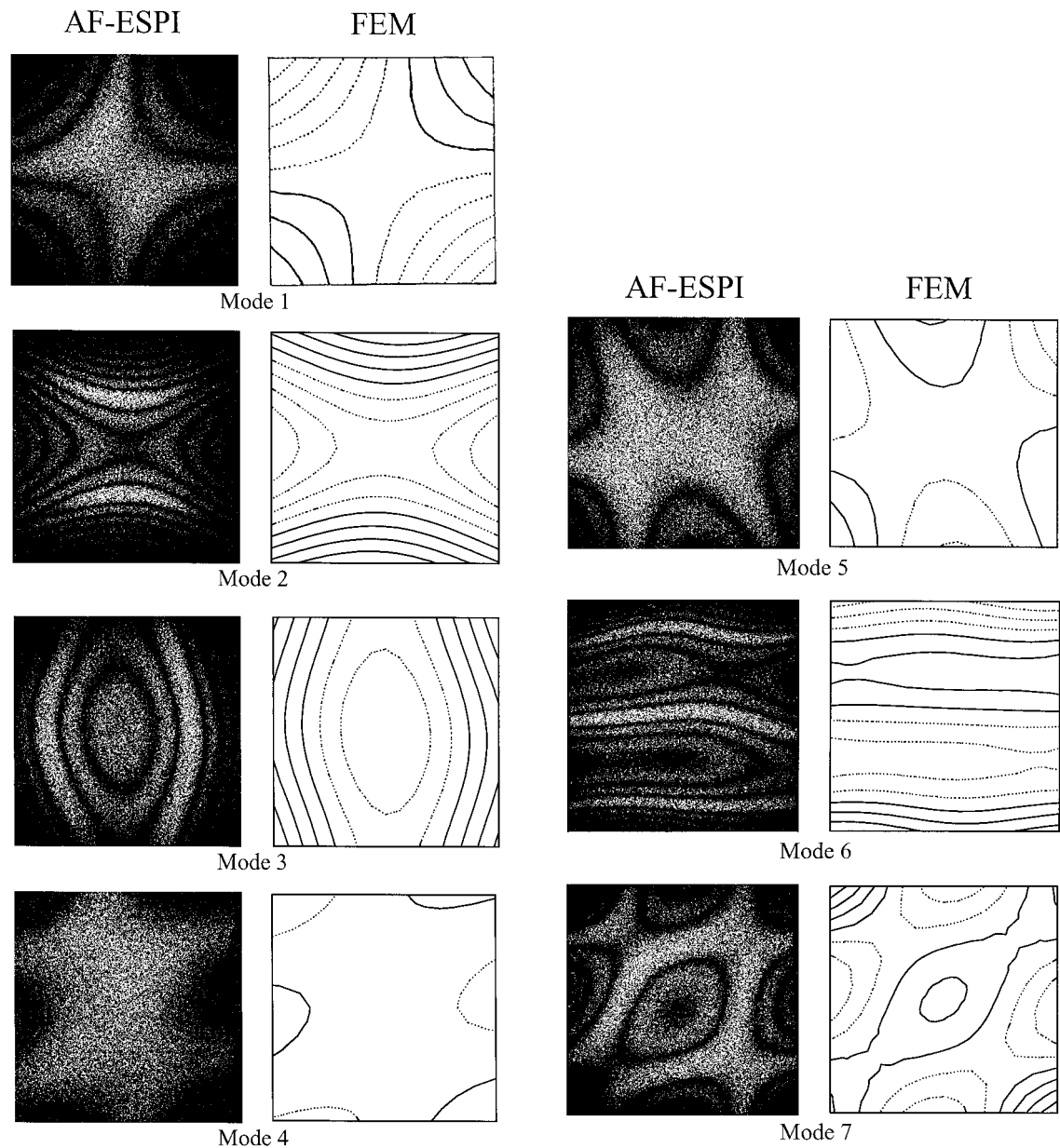

Mode 5

Mode 6

Mode 7

Fig. 5   First seven mode shapes for $[0/45/90/-45]_{2s}$ composite square plate obtained from experimental observation and numerical calculation.

excited at this frequency, a linear combination of these modes will be obtained in experimental observation, and it is not possible to define uniquely the mode shape of the vibration. The precise nature of the mode produced in the experiment depends on the position and method of excitation. The values for (m, n) are the numbers associated with the transverse half waves in the plate along the horizontal and vertical directions, respectively. In the case in which the nodal lines are straight lines parallel to the coordinate axes, the values (m, n) are reported. In other cases, the modes become complicated. For example, modes 2 and 3 in Fig. 2 correspond to the expressions of $(1, 3) - (3, 1)$ and $(1, 2) + (3, 1)$, respectively.

Next, the composite square and rectangular plates with stacking sequences $[0]_{16}$ and $[0/45/90/-45]_{2s}$, with all edges free, are investigated. The resonant frequencies obtained from the analytical methods and experimental measurements are compared in Tables 4–7. Note that the predicted values of resonant frequencies are based on the effective laminate bending stiffness, as discussed earlier. The differences between the predicted values and the experimental resonant frequencies are possibly due to the errors induced by measuring the resonant frequencies from the AF-ESPI technique, the accuracy of the finite element and Rayleigh–Ritz methods, and the suitability of the method for determination of the effective laminate bending stiffness from the material properties of the lamina. The first few

mode shapes for each plate are computed using the finite element package ABAQUS, and the results are compared with the experimental observation from AF-ESPI, as shown in Figs. 3–6. The first few vibration mode shapes for the square (eight modes) and rectangular (seven modes) composite plates with the stacking sequence $[0]_{16}$ are shown in Figs. 3 and 4, respectively. The vibration mode shapes for the square (seven modes) and rectangular (seven modes) composite plates with the stacking sequence $[0/45/90/-45]_{2s}$ are presented in Figs. 5 and 6, respectively. It can be seen that the mode shapes obtained experimentally are in good agreement with those obtained from the finite element method (FEM). The mode shapes of laminated composite plates are influenced by material properties, boundary conditions, geometry, and the lamination arrangement. The last factor provides the designer with more flexibility optimally to synthesize the characteristics (i.e., the stiffness, the fundamental frequencies, and the corresponding mode shapes) of the designed structures. The mode shapes of laminated plates have some particular characteristics that are different from isotropic plates. This is noticed in the case of an orthotropic square plate with the stacking sequence $[0]_{16}$, where the $(1, 3)$, $(2, 3)$, $(1, 4)$, and the $(2, 4)$ modes are found to be associated with frequencies that are lower than the $(3, 1)$ mode. This feature can be explained by comparing the structural properties, boundary conditions, and dimensions of the plate

AF-ESPI   FEM

Mode 1

Mode 2

Mode 3   (3,2)

Mode 4

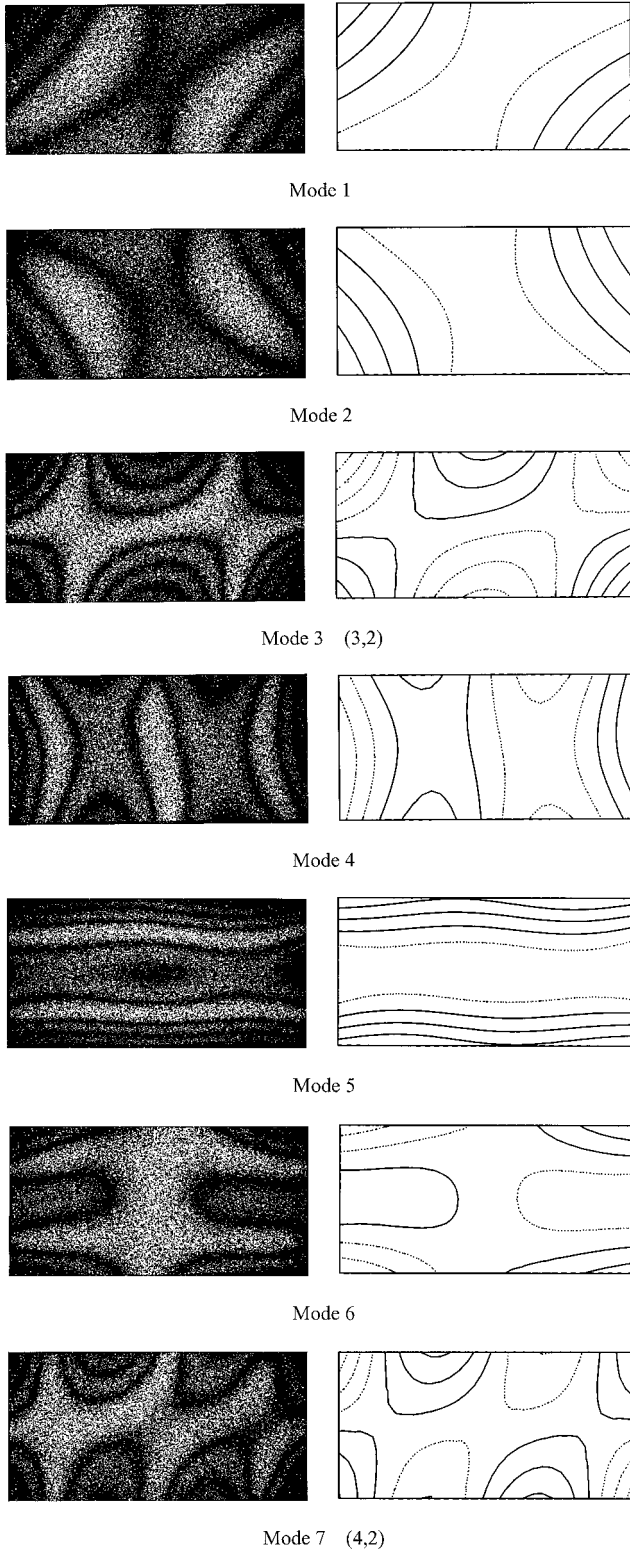

Mode 5

Mode 6

Mode 7   (4,2)

Fig. 6   First seven mode shapes for $[0/45/90/-45]_{2s}$ composite rectangular plate obtained from experimental observation and numerical calculation.

in the x and y directions. For the orthotropic plate, the overall bending stiffness with respect to the y direction is weaker than in the x direction. Therefore, the plate tends to form nodal lines in the y direction first. In contrast, an isotropic square plate has the same frequency for both the (3, 1) and the (1, 3) modes. Making use of the resonant frequencies and vibration mode shapes obtained by the AF-ESPI optical system, an inverse algorithm is developed by the authors.[15]

Conclusions

Optical techniques have been shown to have certain advantages for vibration analysis and ESPI has been applied to many vibration problems. The advantages of the optical ESPI method include noncontact and full-field measurement, real-time observation, submicron sensitivity, validity of both static deformation and dynamic vibration, and direct digital image output. Because ESPI uses video recording and display, it works in real time to measure dynamic displacement, which makes it possible to implement this technique for vibration measurement. A self-arranged AF-ESPI optical setup with good visibility and noise reduction has been used in this study to obtain the resonant frequencies and the corresponding mode shapes of free vibration of laminated composite plates at the same time. Compared with the spectrum analysis or modal analysis method, AF-ESPI is more convenient in experimental operation. Two different types of stacking sequences and two plate geometries are investigated in this study, and an acceptable quality of mode shapes is generated using the experimental optical interferometry method. Numerical calculations of resonant frequencies and mode shapes based on a finite element package and a Rayleigh–Ritz method are performed, and good agreements are obtained when compared with experimental measurements. The results shown in this study demonstrate that the prediction of the resonant frequencies and mode shapes of composite plates is applicable by using the effective material constants from an averaging process.

References

[1]Rastogi, P. K., *Holographic Interferometry*, Springer-Verlag, Berlin, 1994.

[2]Butters, J. N., and Leendertz, J. A., "Speckle Pattern and Holographic Techniques in Engineering Metrology," *Optics Laser Technology*, Vol. 3, No. 1, 1971, pp. 26–30.

[3]Jones, R., and Wykes, C., *Holographic and Speckle Interferometry*, Cambridge Univ. Press, Cambridge, England, U.K., 1989, pp.165–196.

[4]Løkberg, O. J., and Hogmoen, K., "Use of Modulated Reference Wave in Electronic Speckle Pattern Interferometry," *Journal of Physics. E: Scientific Instruments*, Vol. 9, 1976, pp. 847–851.

[5]Creath, K., and Slettemoen, G. A., "Vibration-Observation Techniques for Digital Speckle-Pattern Interferometry," *Journal of the Optical Society of America A*, Vol. 2, No. 10, 1985, pp. 1629–1636.

[6]Pouet, B., Chatters, T., and Krishnaswamy, S., "Synchronized Reference Updating Technique for Electronic Speckle Interferometry," *Journal of Nondestructive Evaluation*, Vol. 12, No. 2, 1993, pp. 133–138.

[7]Wang, W. C., Hwang, C. H., and Lin, S. Y., "Vibration Measurement by the Time-Averaged Electronic Speckle Pattern Interferometry Methods," *Applied Optics*, Vol. 35, No. 22, 1996, pp. 4502–4509.

[8]Ma, C. C., and Huang, C. H., "The Investigation of Three-Dimensional Vibration for Piezoelectric Rectangular Parallelepipeds by Using the AF-ESPI Method," *IEEE Transactions on Ultrasonics, Ferroelectrics, and Frequency Control* (to be published).

[9]Huang, C. H., and Ma, C. C., "Vibration Characteristics for Piezoelectric Cylinders Using Amplitude-Fluctuation Electronic Speckle Pattern Interferometry," *AIAA Journal*, Vol. 36, No. 12, 1998, pp. 2262–2268.

[10]Young, D., "Vibration of Rectangular Plates by the Ritz Method," *Journal of Applied Mechanics*, Vol. 17, No. 4, 1950, pp. 448–453.

[11]Leissa, A. W., "The Free Vibration of Rectangular Plates," *Journal of Sound and Vibration*, Vol. 31, No. 3, 1973, pp. 257–293.

[12]*ABAQUS User's Manual*, Ver. 5.5, Hibbit, Karlsson, and Sorensen, Inc., Pawtucket, RI, 1995.

[13]Huang, C. H., and Ma, C. C., "Experimental Measurement of Mode Shapes and Frequencies for Vibration of Plates by Optical Interferometry Method," *Journal of Vibration and Acoustics* (to be published).

[14]Slangen, P., Berwart, L., de Veuster, C., Golinval, J. C., and Lion, Y., "Digital Speckle Pattern Interferometry (DSPI): A Fast Procedure to Detect and Measure Vibration Mode Shapes," *Optics and Lasers in Engineering*, Vol. 25, No. 5, 1996, pp. 311–321.

[15]Ma, C. C., and Lin, C. C., "Inverse Evaluation of Material Constants for Composite Plates by Optical Interferometry Method," *AIAA Journal*, Vol. 37, No. 8, 1999, pp. 947–953.

A. Berman
Associate Editor